©*Proc. Indian natn. Sci. Acad.*, **52**, A, No. 1, 1986, pp. 232–264.
Printed in India.

METAL-INSULATOR TRANSITIONS IN THE V_2O_3 ALLOY SYSTEM : EXPERIMENT AND THEORY*

J M HONIG *and* J SPAŁEK**

Departments of Chemistry and Physics, Purdue University; West Lafayette, Indiana 47907, USA

(*Received 6 December 1985*)

A review is provided of a recent theory pertaining to properties of correlated electron systems, with particular application to the V_2O_3 alloy system. Correlation effects are introduced by specification of a parameter U/W, the ratio of intrasite Coulomb energies to bare-particle bandwidths. Under suitable conditions, a metal-insulator transition and its inverse may be brought about by increasing the temperature at fixed U/W. The conditions for bringing about reentrant metallic behaviour are specified in an appropriate phase diagram. The theory is then expanded to take into account transitions that occur at low temperature as a concomitant to the onset of antiferromagnetic order. Numerical results based on the above theory are compared with experimental work reported for the $(V_{1-x}Cr_x)_2O_3$ sytstem; the results are in semi-quantitative agreement. It is pointed out that lattice effects must be included for a better description of the various metal-insulator transitions observed in this system.

Key Words : Electron, V_2O_3 Alloy and $(V_{1-x}Cr_x)_2O_3$ Systems; Correlation Effects; Conlomb Energy; Bare-Particle Bandwidths; Metal-Insulator Transitions

I. HISTORICAL INTRODUCTION

THE V_2O_3 system and its alloys with several transition metal oxides has been the subject of approximately 500 investigations ever since the report by Foëx[1] of a phase transformation in V_2O_3 at 173 K. His dilatometric and resistivity measurements on compacted powder specimens were later confirmed by Morin[2] who reported on the electrical conductivity of V_2O_3 single crystals. Feinleib and Paul[3] extended these measurements to higher temperatures where they encountered an additional resistivity anomaly in the range 350–650 K (see Fig. 1*c*). MacMillan[4] in an unpublished report first showed that a more complex set of transitions is exhibited by the $(V_{1-x}Cr_x)_2O_3$ alloy system in the range $0 < x < 0.1$. These studies were then continued by workers at Bell Laboratories[5–7] who reported on the occurrence, with rising temperature, of an insulator-metal transformation in the range $25 < T_1 < 180$ K, and of a second metal-insulator transition in the range $180 < T_2 < 350$ K; the T_1 and T_2 values vary with x. The Bell group[8,9] also studied the effects of incorporating Al_2O_3, Ti_2O_3, Fe_2O_3, and other transition metal oxides into V_2O_3; they

*Presented at the INSA Golden Jubilee Symposium on Solid State Chemistry held at INSA, New Delhi during December 4-6, 1985.

****Permanent Address** : Dr Jozef Spalek, Zaklad Fizyki Ciala Stalego, AGH, Al Mickiewicza 30, PL-30-059 Kraków, Poland.

and others[10,11] further initiated a study of the changes in physical properties as the oxygen/metal ratio is altered. The Purdue research group[12a,12b,13,14] enlarged on the earlier findings by reporting still another insulator-metal transition in the $(V_{1-x}Cr_x)_2O_3$ alloy system for $x > 0.005$ over a wide temperature range T_3 above 350 K, thus showing that such alloys exhibit reentrant metallic behavior. These later investigators also directed attention to sizeable hysteresis effects at T_1 and T_2, and systematized the effects of incorporating Cr, Al, or Ti cations and cation vacancies. An enormous number of additional publications in the period 1945–85 has dealt with many other types of physical measurements on the above systems; for a dated review see Honig and Van Zandt.[12]

The current status of the field is perhaps best summarized in terms of Figs. 1(*a*)-(*e*) in which the resistivity ρ is plotted logarithmically against inverse temperature, T^{-1}. These schematic diagrams show a number of interesting features : For the V_2O_3 (98.5 per cent)-Cr_2O_3 (1.5 per cent) system one encounters the three transitions sketched out in Fig. 1(*a*). In the range between 0 and $\sim$ 150 K the alloy is an antiferromagnetic insulator (AFI). There occurs a sharp transformation to the paramagnetic metallic state (PM) which prevails between $\sim$ 150 and $\sim$ 300 K. At that point another first order transition carries the system to a paramagnetic insulating state (PI). In the range $\sim$ 300–1000 K the resistivity gradually diminishes with rising temperature, so that beyond $\sim$ 650 K the alloy system is in a high temperature paramagnetic metallic phase (PM′) which closely resembles the PM configuration. This three-transition pattern may be readily altered by slight changes in alloying. The electrical properties of the V_2O_3 (97 per cent)-Cr_2O_3 (3 per cent) alloy system are sketched out in Fig. 1(*b*). It is seen that the PM phase is eliminated altogether; on heating, the alloy proceeds directly from the AFI to the PI configurations via a sharp ($x = 0.02 - 0.03$) or rounded ($x > 0.03$) transition; this is followed by a gradual changeover to the PM′ state. In pure V_2O_3 the electrical resistivity exhibits yet a different pattern : as shown in Fig. 1(*c*), there is a large, first-order transition near 150 K which links the AFI and PM phases. With rising temperatures in the range 350-650 K an anomalous rise in resistivity takes place, so that undoped or lightly Cr_2O_3-doped V_2O_3 passes continuously from the PM to the PM′ configuration. Fig. 1(*d*) sketches the situation for V_2O_3 (99 per cent)-Ti_2O_3 (1 per cent) and for nonstoichiometric V_2O_3. Basically, the AFI—PM transition is shifted to lower temperature and the resistivity discontinuity diminishes or increases with increasing Ti or cation vacancy content. Finally, as sketched in Fig. 1(*e*), when the Ti content is increased beyond 5.5 at per cent or the vacancy concentration passes beyond 0.9 at. per cent all transitions are eliminated and only the PM phase is retained. However, below approximately 10–15 K the metallic phase transforms to an antiferromagnetic metal (AFM).[13a] A phase diagram which summarizes the stability domains of the various phases is exhibited in Fig. 2, and the actual electrical resistivity measurements on which this diagram is based are displayed in Fig. 3(*a*), (*b*), and (*c*). The experimental work and the various features of the data have been explained elsewhere[14,15] in great detail; this commentary will not be repeated here. Instead, we concentrate on the theoretical analysis of the

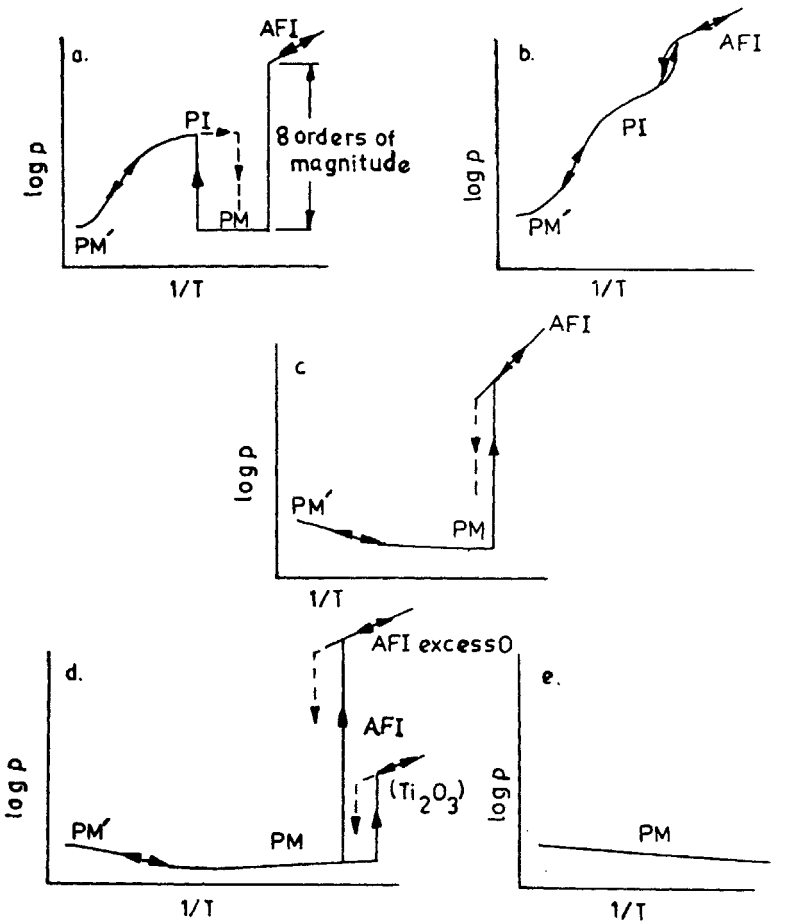

FIG 1 Schematic diagram depicting the changes of resistivity ρ with temperature T for the V_2O_3 alloy system. Part (*a*) : $(V_{1-x}Cr_x)_2O_3$ with $0.005 < x < 0.018$; note the three transitions AFI → PM → PI → PM′ with rising T and the large hysteresis involved in the PM → PI transformation. Part (*b*) : $(V_{1-x}Cr_x)_2O_3$ with $x > 0.018$; the metallic PM phase is now bypassed. Part (*c*) : Undoped V_2O_3; the PM–PI transition is bypassed. Part (*d*): $(V_{1-x}Ti_x)_2O_3$ for $0 < x < 0.055$ and $(V_{1-y}\square_y)_2O_3$ $0 < y < 0.009$; this situation is similar to part (*c*) but the transition is shifted to lower temperatures and the size of the AFI—PM discontinuity in log ρ is altered. Part (*e*): $(V_{1-x}Ti_x)_2O_3$ for $x > 0.055$ and $(V_{1-y}\square_y)_2O_3$ for $y > 0.009$; the alloys remain metallic.

rather complex set of transitions. The principal feature of interest is the fact that a causal factor as small as thermal energy change of the order of k_BT (where k_B is the Boltzmann constant and T, the temperature) can bring about repercussions that are all out of proportion to the stimulus. It will be our task to explore these matters in the subsequent sections. In particular, we focus on the problem of rationalizing the observed reentrant metallic behaviour of the $(V_{1-x}Cr_x)_2O_3$ alloys with $0.005 < x < 0.018$.

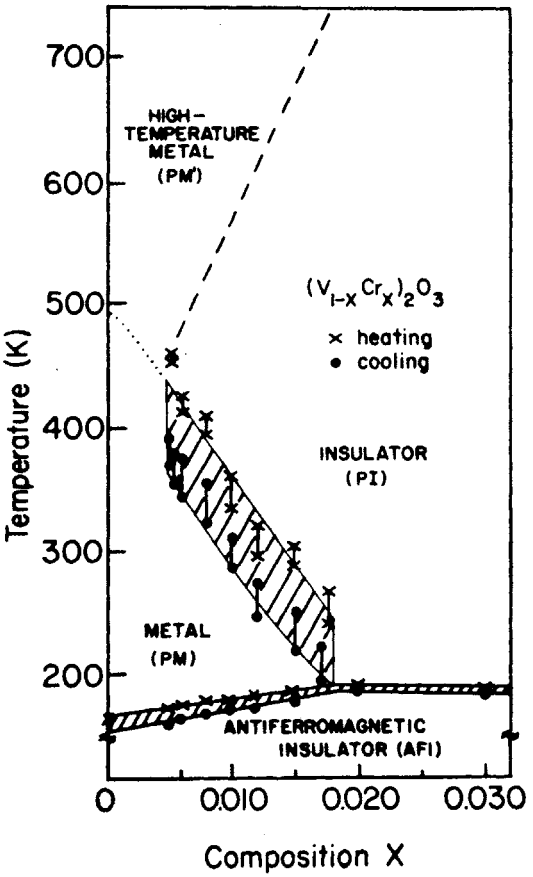

FIG 2 Experimental phase diagram for the $(V_{1-x}Cr_x)_2O_3$ alloys system. Hatched areas show ranges of hysteretic effects. Dotted line separating PM and PM′ regions is drawn at midpoint of the gradual transition.

II THEORETICAL INTERPRETATION

A. Historical Survey

There have been many attempts to explain the rich variety of transitions encountered in the V_2O_3 alloy systems. In many instances models were proposed before an adequate data base had become available, and a number of such descriptions are no longer tenable.

Many of the proposed mechanisms are couched in rather equalitative terms. Among these are the adoption by the Bell group[5,9] of electron correlations as the principal driving mechanism for one or more of the observed tranformations; thus the several phase changes were classified by them as examples of the Mott transition.[15–19] On the other hand, the Purdue group[14,15] has pointed to unmistakable signs that the lattice also plays an important role in the transitions; they inter-

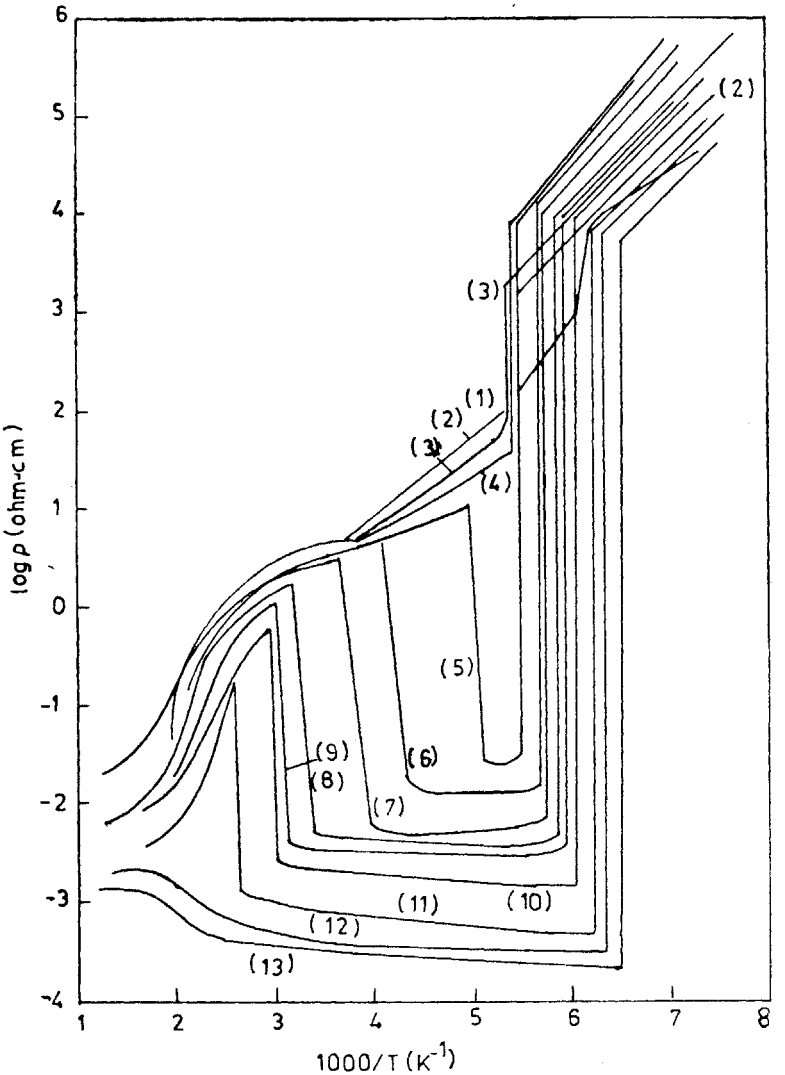

FIG 3 Experimental measurements pertaining to the variation of resistivity ρ with temperature T for the V_2O_3 alloy system. Part (*a*): $(V_{1-x}Cr_x)_2O_3$ with $0 \leqslant x \leqslant 0.1$; note the varying number of metal-insulator transitions for the regimes $0 \leqslant x < 0.005$, $0.005 < x < 0.018$, and $0.018 < x < 0.010$.

preted their data in terms of the density-of-states [DOS] diagram peculiar to the states of primarily *d*-character in V_2O_3.[14] They emphasized that the Fermi level was situated in a deep minimum of the DOS, which can be opened up and closed again by small perturbations on the system.

In a later Section, we will present a theory that in a sense mediates between these opposing views and which seems to provide a more adequate interpretation of the experimentally observed phase diagram of Fig. 2.

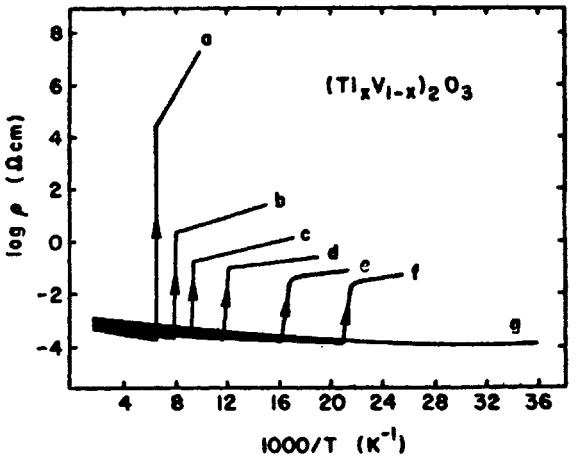

FIG 3 Part (*b*) : $(V_{1-x}Ti_x)_2O_3$ for $0 < x < 0.015$; note the reduction in conductivity activation energy and the diminution of the resistivity discontinuity with increasing x.

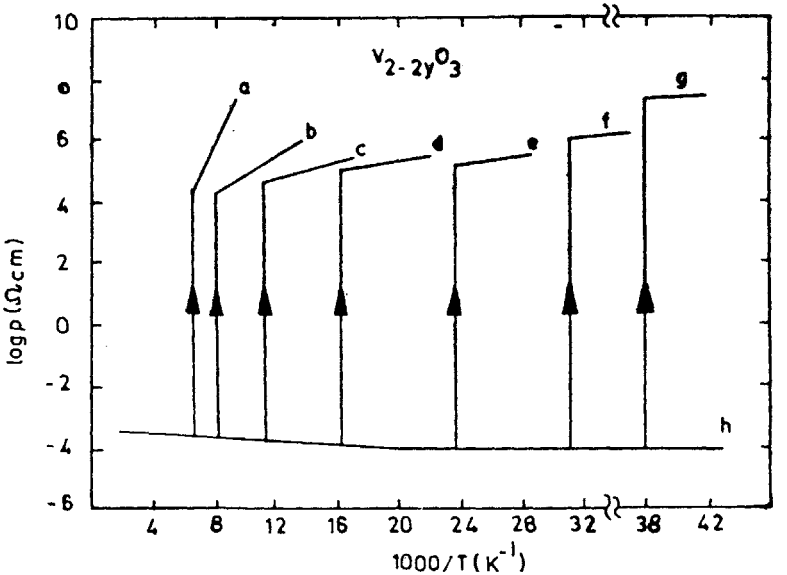

FIG 3 Part (*c*) : $(V_{1-y}y)_2O_3$ note the variation of conductivity activation energy and of the discontinuity in resistivity with increasing y.

Aside from the above qualitative formulations, several quantitative theories have been advanced. Among these is the treatment by Brinkman and Rice[21]; they studied the mechanism of metal-insulator transitions at the absolute zero of temperature ($T = 0$) in terms of electron correlation effects whose strength was specified by the ratio U/W, where U is the intra-atomic Coulomb repulsion energy for the electrons situated on the same lattice site, and W is the bare-particle band width. This theory applies to phenomena as observed when one moves along the abscissa

of the phase diagram in Fig. 2 at $T = 0$, but which was not extended to the regime of non-zero temperature. The Brinkman-Rice analysis, therefore, is primarily applicable to experiments in which either the concentration of additives to the V_2O_3 host is altered or in which pressure changes are studied; as shown later, both these effects scale roughly linearly with U/W. It may also be shown[22] that the above theoretical formulation is recovered as a special case of the treatment described below.

Several theories, describing the phase transitions of V_2O_3 at non-zero temperatures have also been published. Cyrot[23,24] constructed a phase diagram that summarized the various transition anticipated for the system. To obtain first-order transformations he found it necessary to include a volume-dependence of the bare bandwidth W, in addition to magnetic spin fluctuations. His phase diagram in the k_BT/W *vs.* U/W plane is only in rough conformity with the various phases experimentally detected in the V_2O_3 system. Moriya and Hasegawa[25] as well as Hasegawa[26] have applied spin fluctuation theory to the problem; they did not obtain any first-order transition, which fact they attributed to neglect of lattice effects.

As an alternative, Zeiger[27] proposed a theory in which electron correlation effects compete against the entropy of electrons in band states. He allowed the one electron energies to depend on interatomic separations. The five parameter theory and specification of density-of-state (DOS) functions for two bands can explain a large variety of experimental results in the V_2O_3 alloy system but is less successful in dealing with detailed electrical properties.

Several theories of the band structure for the V_2O_3 alloy systems have also been published.[28–31] While differing in detail all treatments yield DOS curves for the d-band in which sharp peaks and deep valley alternate. In such circumstances, if the Fermi level coincides with a valley, small external perturbations such as magnetic ordering effects, application of pressure, changes in temperature, and variations in alloy-composition are sufficient to open up or close a band-gap that takes the place of the minimum in the DOS curve. In these models correlation effects play a somewhat subsidiary role, but they are still manifest in the small widths of the subbands.

Another approach was introduced simultaneously by Minesaki,[32] Ramirez *et al.*[33] and by Alascio *et al.*[34] who essentially adapted the order-disorder theory, as elaborated upon by Falicov and Kimball[35] to electrons and holes in localized and itinerant states. These authors calculated the fraction of carriers available for electrical conduction as a function of temperature in terms of an electron-hole interaction energy parameter; they found a very sharp change in carrier density with temperature, beyond a critical value of the interaction energy. This is a manifestation of the metal-insulator transition. The latter is driven jointly by the electron-hole interactions, by the configurational entropies arising from the distribution of electrons among the two levels of each lattice site, and by alterations in magnetic spin entropy resulting from changes in electron population on each site. The principal difficulty with this approach is that, without further modification, it does not provide an explanation of the reentrant metallic behaviour encountered in the V_2O_3 alloy system.

We now present in outline form a recent theoretical development[22,36] that mediates between the strongly correlated electron limit and freely itinerant electron behaviour. As will be seen, the simple approach developed here rather successfully deals with the observed variety of electrical properties of the V_2O_3 alloy system; however, lattice effects which have been neglected must be built in at a later stage to obtain a more satisfactory representation of experimental data.

III Elementary Description of the Correlated Paramagnetic Regime

A. Preliminaries

The task of providing a theoretical framework for interpreting the reentrant metallic characteristics of the V_2O_3 alloy system will be attended to in several stages of increasing complexity. We recognize at the outset that even in the metallic phase electrons in bands of primarily *d*-character are strongly correlated; this interaction must be included in the expressions for both the band (kinetic) energy of the charge carriers and for the potential interaction energies. To simplify the analysis we assume that electrons are accommodated in a single, non-degenerate band that is exactly half-filled; we, later, specialize to the limiting case of low temperatures ($T \to 0$). Our approach is to provide first a phenomenological description of the electronic states by deriving expressions for the Helmholtz free energy F of the charge carriers either in the paramagnetic metallic (PM) or in the paramagnetic insulating (PI) regimes. A transition between these states is achieved when the coexistence line $F_{PM} = F_{PI}$ is crossed in either direction by alteration of temperature or of sample composition.

B. The Potential Energy of Interaction in the Metallic Regime

The potential interaction energy among correlated electrons will be handled in a very elementary manner along the lines suggested by Hubbard.[20] The charge carriers are treated as non-interacting unless two of them settle on the same lattice site with opposing spins, in which case their interaction energy is set equal to U. The total potential energy is thus given by $U\eta$, where η is the expectation value $\langle n_{j\uparrow} n_{j\downarrow} \rangle$ for encountering a typical site in a doubly occupied state, involving two electrons with opposing spins. In the PM regime $\langle n_{j\uparrow} \rangle$ and $\langle n_{j\downarrow} \rangle$ are assumed to be independent of the site index j.

C. The Kinetic Energy of the Correlated Electron Gas

The potential energy of interaction described above also produces a hindered motion whenever the charge carriers attempt to get past each other. An elementary technique for dealing with this problem is to construct a set of independent quasiparticles of band energy E that take the place of the interacting electrons. The central *ansatz* in the present theory is that the energy of quasiparticles E is related to the bare particle energy ϵ by a universal scaling law of the form $E = \Phi(\eta)\epsilon$, where the factor Φ depends functionally on η but is independent of temperature T. The rationale for such a step is explained elsewhere[22] in some detail, but ultimately its adoption can only be justified by the degree of success one achieves in dealing with

complicated experimental observations. The band energy of the N quasiparticles may now be written as

$$\frac{E_B}{N} = \int_{-\infty}^{\infty} Ef(E)\rho(E)\,\mathrm{d}E, \qquad \ldots(1)$$

where $f(E) \equiv f[(E - E_F)/k_BT]$ is the Fermi-Dirac distribution function for the quasiparticles (E_F is the Fermi energy), and $\rho(E)$ is the appropriate density-of-states (DOS) function. Next, introduce the scaling law; one then finds that $f(E) \equiv f[(E - E_F)/k_BT] = f[\Phi(\epsilon - \mu)/k_BT] = f[(\epsilon - \mu)/k_BT^*] \equiv f^*(\epsilon)$ in which we have set $\mu \equiv E_F/\Phi$ as the Fermi energy for bare particles and $T^* \equiv T/\Phi$ as an *effective temperature*. As regards the DOS, by definition, $\rho(E)$ is proportional to a set of Dirac delta distributions $\delta(E - E_{\mathbf{k}})$ centered on each of the allowed eigenvalues $E_{\mathbf{k}}$ of the quasiparticle energy spectrum. Thus,

$$N\rho(E) = \sum_{\mathbf{k}} \delta(\Phi(\epsilon - \epsilon_{\mathbf{k}})) = \sum_{\mathbf{k}} \Phi^{-1}\delta(\epsilon - \epsilon_{\mathbf{k}}) = \Phi^{-1}(\eta)\rho_0(\epsilon)N; \qquad \ldots(2)$$

that is, the DOS for the quasiparticle $\rho(E)$ and bare particle systems $\rho_0(\epsilon)$ are related by the scaling factor Φ. Lastly, we replace E and $\mathrm{d}E$ in terms of ϵ and $\mathrm{d}\epsilon$. Eq. (1) thus becomes

$$\frac{E_B}{N} = \Phi \int_{-W/2}^{W/2} \epsilon f^*(\epsilon)\rho_0(\epsilon)\,\mathrm{d}\epsilon \equiv \Phi(\eta)\bar{\epsilon}(T^*) \qquad \ldots(3)$$

We see that the band energy for a set of quasiparticles (and through the ansatz, the interacting electron system) can be handled by introducing the kinetic energy of an equivalent set of noninteracting electrons at an effective temperature T^*, multiplied by a band-narrowing factor $\Phi < 1$ (see below).

D. The Energy of the Correlated Electron System in the Paramagnetic Regime

We next combine the preceding results to obtain a total band energy in the form

$$\frac{E_{PM}}{N} = \Phi(\eta)\bar{\epsilon}(T^*) + U\eta \qquad \ldots(4)$$

It is now necessary to specify the functional form $\Phi(\eta)$. This problem has been dealt with elsewhere[22] and will not be discussed in detail. For a half-filled band, $\eta \leqslant 1/4$; one, therefore, assumes that Φ may be expanded in a Taylor series of the form $\Phi = f_0 + f_1\eta + f_2\eta^2 + \ldots$, the f_i multipliers are then found by requiring E_{PM} to coincide with certain limiting cases for which the total energy is well established. This procedure leads to the simple expression, valid for a half-filled band,

$$\Phi(\eta) = 8\eta(1-2\eta) \qquad \ldots(5)$$

Finally, to explore the low-temperature limiting value of E_{PM} we adopt the featureless DOS of rectangular character : for $-W/2 \leqslant \epsilon \leqslant W/2$, $\rho_0(\epsilon) = 2/W$;

outside this range $\rho_0(\epsilon)$ vanishes. Then for a half-filled band we can set $f^*(\epsilon) = 1$ inside the range $-W/2 \leqslant \epsilon \leqslant 0$ and set $f^*(\epsilon) = 0$ elsewhere. For this case eq. (2) yields $\bar{\epsilon}(0) = -W/4$, so that

$$\frac{E_{PM}}{N} = -\left(\frac{W}{4}\right)\Phi + U\eta \qquad \ldots(6)$$

Consistent with the limit of low temperatures and the use of quasiparticles that obey Fermi-Dirac statistics we now adopt the Sommerfeld approximation for the electronic heat capacity C of the quasiparticles :

$$C = \gamma(E_F)T; \qquad \gamma = \tfrac{2}{3}\pi^2\rho^*(E_F) = \tfrac{2}{3}\frac{\pi^2\rho_0^{\sigma}(\epsilon)}{\Phi}k_B^2 \equiv \frac{\gamma_0}{\Phi}, \qquad \ldots(7)$$

where we have introduced the Sommerfeld constant γ for the quasi-particles and then transformed to the expression γ_0 appropriate to bare particles. The energy and entropy are now given as

$$\frac{E_{PM}(T)}{N} = -\left(\frac{W}{4}\right)\Phi + U\eta + \int_0^T CdT = -\left(\frac{U}{W}\right)\Phi + U\eta + \frac{\gamma_0 T^2}{2\Phi} \qquad \ldots(8a)$$

and

$$\frac{S_{PM}(T)}{N} = \int_0^T \left(\frac{C}{T}\right)\mathrm{d}T = \frac{\gamma_0 T}{\Phi}. \qquad \ldots(8b)$$

E. The Free Energy Functionat for the Correlated Metallic Phase and its Minimization

One may now construct the Helmholtz free energy functional as $F_{PM} = E_{PM} - TS_{PM}$; from (8) one finds

$$\frac{F_{PM}}{N} = -\left(\frac{W}{4}\right)\Phi + U\eta - \tfrac{1}{2}\frac{\gamma_0 T^2}{\Phi} \qquad \ldots(9)$$

It should be carefully noted that the above is not the Helmholtz free energy, because it contains the extrathermodynamic variable η and the function $\Phi(\eta)$ thereof. We thus utilize the Landau technique by minimizing F_{PM} with respect to η using eq. (5). The condition $(\partial F_{PM}/\partial\eta) = 0$ in the limit $T \to 0$ yields

$$\eta = \eta_0 = \tfrac{1}{4}\left(1 - \frac{U}{2W}\right) \qquad \ldots(10a)$$

$$\Phi = \Phi_0 = 1 - \left(\frac{U}{2W}\right)^2 \qquad \ldots(10b)$$

and when these quantities are inserted in (9) one obtains the final result

$$\frac{F_{PM}}{NW} = -\frac{\Phi_0}{4} + \frac{U}{W}\eta_0 - \frac{\gamma_0 T^2}{2\Phi_0 W} \qquad \ldots(11)$$

Actually, we have been slightly inconsistent in the above approach : we should have retained in eqs. (10*a*) and (10*b*) terms up to order T^2, before substituting the expanded expressions for η and Φ into eq. (9). However, it turns out that these higher order terms simply cancel out in the final subtitution, so that eq. (11) is again recovered when a self-consistent procedure is adopted. The Helmholtz free energy for the paramagnetic phase thus consists of a temperature-independent term associated with the energy

$$\frac{E}{NW} = -\frac{\Phi_0}{4} + \frac{U}{W}\eta_0 = -\tfrac{1}{4}\left(1 - \frac{U}{2W}\right)^2 \equiv J, \qquad \ldots(12)$$

and of a temperature-dependent portion $-\gamma_0 T^2/2\Phi_0 W$ associated with the $-TS/NW$ contribution to F/NW.

F. The Free Energy for the Paramagnetic Insulating Phase

We turn now to the formulation of the free energy for the paramagnetic insulating phase. For $n = 1$ the ground state achieved in the low-temperature limit is a distribution of one localized carrier on each site. The energy of this collection coincides with the midpoint of the non-degenerate band described above, i.e. with the assumed zero of energy. Since there are essentially no double occupancies, the repulsive potential energy also vanishes. This leaves only the entropy of the system, given by $Nk_B \ln 2$, since at any given site the electron spin can be in either the spin-up or the spin-down configuration.

Accordingly, the reduced Helmholtz free energy per particle is given by

$$\frac{F_{PI}}{NW} = -\left(\frac{k_B T}{W}\right)\ln 2 \qquad \ldots(13)$$

G. Coexistence Conditions and Phase Diagrams

One can now inquire under what conditions a phase transition from the PM to the PI configuration or its reverse may be achieved. For this purpose one must cross the coexistence line which is defined by the constraint that the chemical potential of the two phases be the same. One must thus set $F_{PM}/NW = F_{PI}/NW$; on equating eqs. (11) with (13) one obtains a quadratic equation in $k_B T/W$ which may be solved for its two roots

$$\left(\frac{k_B T}{W}\right)_{\pm} = \frac{k_B^2 \Phi}{\gamma_0 W}\left\{\ln 2 \pm \left[(\ln 2)^2 - \frac{2\gamma_0}{k_B^2}\left(\frac{W}{4} - \frac{U}{\Phi_0}\eta_0\right)\right]^{1/2}\right\} \qquad \ldots(14)$$

On substituting for γ_0, Φ_0, η_0 and setting $\rho_0^{\sigma} = \frac{1}{W}$ for the featureless DOS for a particle of specified spin σ, we finally obtain

$$\left(\frac{k_B T}{W}\right)_{\pm} = \frac{3}{2\pi^2}\left[1 - \left(\frac{U}{2W}\right)^2\right]\left\{\ln 2 \pm \left[(\ln 2)^2 - \frac{\pi^2}{3}\frac{(1 - U/2W)}{(1 + U/2W)}\right]^{1/2}\right\} \qquad \ldots(15)$$

Eq. (15) forms the basis for the construction of the phase diagram in the low-temperature limit, for the case $n = 1$, and for a featureless DOS. The diagram is shown in Fig. 4 as a plot of k_BT/W *vs.* U/W. Several features are of interest: There is a lower limit, $(U/W)_1$ below which only the PM phase is encountered at all temperatures. The value $(U/W)_1$ represents the point at which the two solution branches $(k_BT/W)_+$ and $(k_BT/W)_-$ coalesce. The lower branch, $(k_BT/W)_-$ drops away from the coalescence point and reaches zero at $U/W = 2$ on the abscissa. The upper branch rises away from the coalescence point; we have arbitrarily cut it off well below the value $U/W = 1.765$ which is a true, atomatic cut-off point in the more sophisticated approach cited below. One must remember that for reduced temperatures k_BT/W considerably in excess of the coalescence point the low-temperature approximation fails, and unphysical predictions ensue if one pushes the theory too far beyond that point.

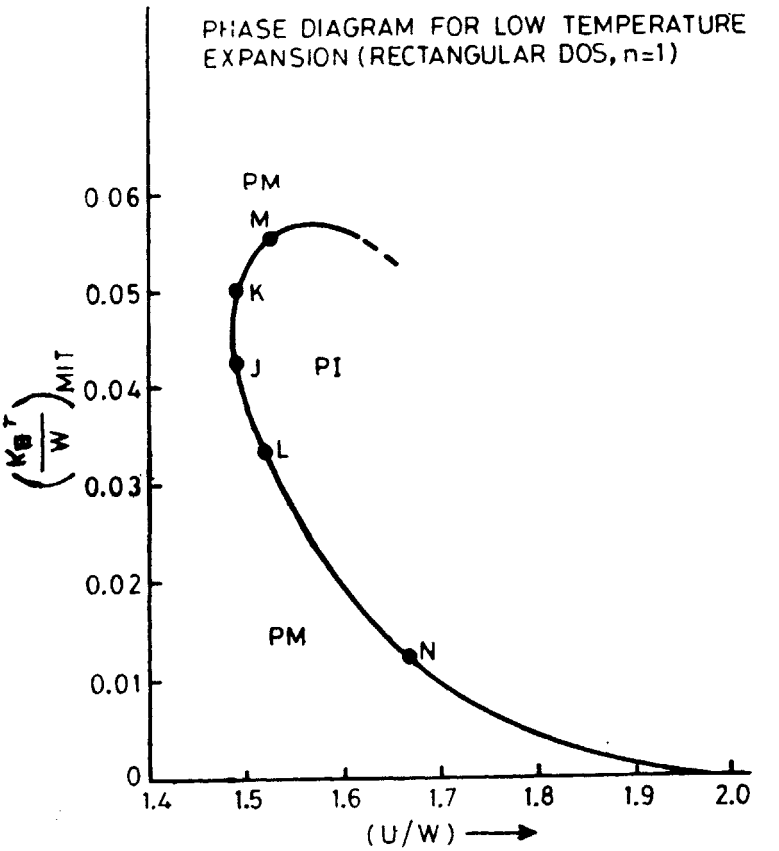

FIG 4 Theoretical phase diagram for the coexistence of metallic and insulating states of a paramagnetic material characterized by a single band that is exactly half-filled. Note the extent of the stability ranges for the PM, PI and PM′ configurations. The phase diagram was determined in the low-temperature limit discussed in the text; the upper critical point is arbitrarily placed as shown (see text). The labels *J, K, L, M, N* correspond to those of Fig. 5.

The origin of the phase diagram may readily be understood by comparing eqs. (11) with (13). The expression for the reduced free energy of the PI phase forms a straight line passing through the origin on a F/NW *vs.* k_BT/W plot, as shown by trace (*e*) in Fig. 5. By contrast, the corresponding expression for the PM phase forms a parabola with a negative intercept J as specified by eq. (12), and a curvature, both of which depend on U and W. For small U/W, i.e. when correlation effects are minor, J is numerically large; the resulting parabola, sketched as curve (*a*) in Fig. 5, everywhere lies below (*e*). The free energy for the PM phase is always less than that of the PI configuration; no transition occurs, and only the mildly correlated metallic phase is encountered. As U/W increases, J becomes numerically smaller and the intercept rises. This ultimately places the parabola up sufficiently high on the ordinate scale that it can cut the straight line (*e*) at two points, denoted by JK or LM for representative curves (*b*) or (*c*) respectively. These intersection points are also marked in Fig. 4. In these circumstances the metallic and insulating phases alternate in exhibiting the lower free energy. As the temperature rises one encounters the progression PM → PI → PM′ which mimics the reentrant metallic feature seen for certain V_2O_3 alloys as described earlier. Finally, as J becomes numerically small the parabola intersects the straight line only at one point N, as illustrated for traces (*d*) and (*e*) in Fig. 5. The second intersection point occurs at unphysical temperatures. Point N is also entered in Fig. 4. In this regime only the PM → PI transformation occurs with rising temperatures.

In summary, a very simple electron correlation model has been proposed to provide a qualitative rationalization of the phase diagram for the paramagnetic configuration of metarials characterized by various values of U/W. It should be

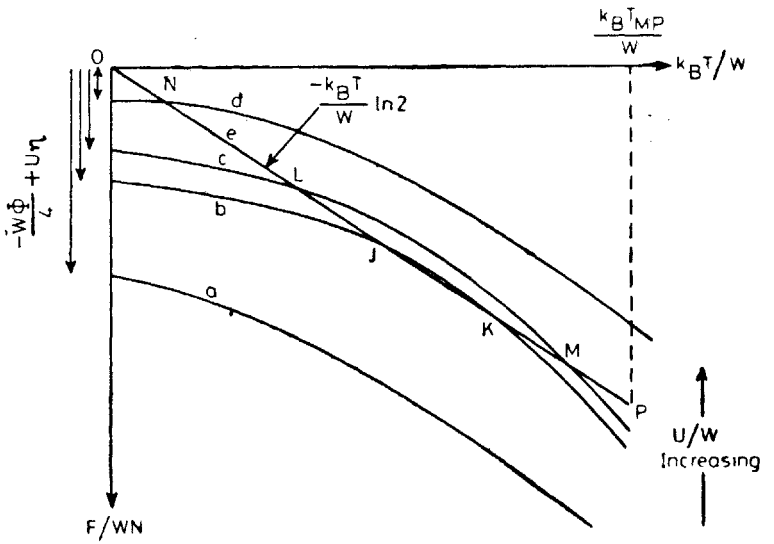

FIG 5 Plots of eqs. (11) and (13) for different values of the U/W parameter. Note the points of intersection *JK*, *LM*, *N* and their counterpart in Fig. 4.

noted that the succession of phases described above is achieved for *fixed* U/W simply by varying the temperature. That such small doses of energy input can achieve such drastic changes in electron configuration is due to the fact that, under conditions where the negative band energies and positive electron correlations nearly balance, the much smaller entropy effects are the deciding factor whether the electrons are in an insulating or metallic state.

We shall defer a comparison between theory and experiment until the more complete theory has been developed below.

IV Improved Theory of Correlated Electron States for Paramagnetic Materials

A. Introductory Comments

The preceding treatment of electron correlation effects is rather primitive and needs to be placed on a sounder theoretical footing. This we accomplish by setting up a theory which deals with the PM or PI phase for both of which itinerant and localized electrons are postulated to coexist. Their ratio must then be adjusted self-consistently by minimizing the functional $F(\eta)$ constructed from the energy and entropy contribution as described below. Naturally, the resulting analysis is now more complex and must ultimately be carried out numerically. By way of compensation we can drop the restriction of operating in the low-temperature limit.

From quite general considerations it may be shown that, for very large intra-atomic repulsion energies U, Φ represents the conditional probability that an electron will execute a transition to a neighbouring site if the latter is empty. For very large U such a transition is prohibited if the neighbouring site is already occupied by another electron. This makes it plausible to associate with Φ the fraction of itinerant electrons, i.e. those capable of executing a transition to other sites; $(1 - \Phi)$ then represents the fraction of electrons hemmed in (i.e. localized) by the lack of available unoccupied nearest neighbor sites. This association holds even for U values which are no longer large compared to bare particle band widths W; in the limit $U \to 0$ the entire question is academic since then all electrons are itinerant.

B. The Energy of the Electron Assembly

To obtain the energy of the electron assembly we proceed in strict analogy to the procedure described in Sec. III C. We replace the interacting electrons, whether itinerant or localized, by a quasiparticle assembly of energy $E_B = \Sigma_{(\mathbf{k})} E_{\mathbf{k}} f(E_{\mathbf{k}})$ where the summation extends over all quantum states occupied by the representative quasiparticles. We then switch to an integration after introducing the DOS $\rho(E)$ and the same scaling law $E = \Phi\epsilon$ as before. This immediately yields

$$\frac{E}{N} = \Phi \int_{-W/2}^{W/2} \epsilon \rho_0(\epsilon) f^*(\epsilon)\, d\epsilon + U\eta \qquad \ldots(16)$$

as the total energy of the interacting electron assembly.

On introducing the explicit form for the Fermi-Dirac function as in Sec. IIIC, we obtain

$$\frac{E}{N} = \Phi \int_{-W/2}^{W/2} \mathrm{d}\epsilon\, \epsilon \rho_0(\epsilon) \tanh\left(\frac{\epsilon}{2k_B T^*}\right) + U\eta \qquad \ldots(17)$$

and on substituting $\rho_0(\epsilon) = 2/W$ and carrying out the integration we find

$$\frac{E}{NW} = \frac{2k_B T}{W}\left\{\int_0^1 \mathrm{d}x \ln\cosh\left(\frac{W\Phi x}{4k_B T}\right) - \ln\cosh\left(\frac{W\Phi}{4k_B T}\right)\right\} + \frac{U\eta}{W} \qquad \ldots(18)$$

The zero of entropy for the electrons has been chosen so as to coincide with the entropy of the localized electron assembly.

C *The Entropy Contribution of the Electron Assembly*

In considering the entropy of electrons we must recognize two distinct contributions : the thermal entropy of mobile carriers, weighted by the factor Φ and the configurational entropy of localized carriers associated with a weighting factor $(1 - \Phi)$.

The entropy of the itinerant electron assembly as represented by the quasiparticles is specified by

$$\frac{S_i}{N} = -\left(\frac{\Phi k_B}{N}\right) \sum_{\mathbf{k}\sigma} \{f(E_{\mathbf{k}}) \ln f(E_{\mathbf{k}}) + [1 - f(E_{\mathbf{k}})] \ln [1 - f(E_{\mathbf{k}})]\} \qquad \ldots(19)$$

On switching to an integration over $E_{\mathbf{k}}$ involving the DOS $\rho(E_{\mathbf{k}})$ and then transforming to the bare particle energies as described earlier we obtain

$$\frac{S_i}{N} = -\Phi k_B \int_{-W/2}^{W/2} \mathrm{d}\epsilon\, \rho_0(\epsilon) \{f^*(\epsilon) \ln f^*(\epsilon) + [1 - f^*(\epsilon)] \ln [(1 - f^*(\epsilon)]\} \qquad \ldots(20)$$

After inserting the expression for $f^*(\epsilon)$ the above expression becomes

$$\frac{S_i}{N} = \Phi k_B \left\{2 \ln 2 - \int_0^{W/2} \mathrm{d}\epsilon\, \rho_0(\epsilon) \left[\frac{\epsilon}{k_B T^*} \tanh\left(\frac{\epsilon}{2k_B T^*}\right) - 2 \ln\cosh\left(\frac{\epsilon}{2k_B T^*}\right)\right]\right\} \qquad \ldots(21)$$

On introducing the usual featureless DOS function we obtain the final relation

$$\frac{S_i}{N} = \Phi k_B \left\{ 2 \ln 2 - 2 \ln \cosh \left(\frac{W\Phi}{4k_BT} \right) + 4 \int_0^1 dx \ln \cosh \left(\frac{W\Phi x}{4k_BT} \right) \right\} \quad \ldots(22)$$

The entropy of the localized electron group is calculated according to the expression

$$\frac{S_1}{N} = (1 - \Phi) k_B \sum_j P_j \ln P_j \quad (j = 0, 1, 2, 3), \quad \ldots(23)$$

where the P_j specify the probability that a given lattice site contains no electron, a localized electron in spin-up or spin-down configuration, or two electrons of opposite spin. The probabilities are listed in Table I; on introducing the condition $\nu_\sigma = \nu_{-\sigma} = \nu/2$ for the paramagnetic regime and the particle conservation law $n = \nu + 2\eta$, the entropy for the localized phase is specified as

TABLE I

Configuration	*Designation*	*Average Probability of Occurrence*
Site Contains Electron with Spin Up: $\sigma = 1$	P_2	ν_σ
Site Contains Electron with Spin Down; $\sigma = -1$	P_3	$\nu_{-\sigma}$
Doubly Occupied Site	P_4	η
Unoccupied Site	P_1	$1 - \nu - \eta$

$$\left(\frac{S_1}{N} \right) = k_B (1 - \Phi) [- (n - 2\eta) \ln (n - 2\eta) + (n - 2\eta) \ln 2 - \eta \ln \eta - (1 - n + \eta) \ln (1 - n + \eta)] \quad \ldots(24)$$

D. The Free Energy of the System

The Helmholtz free energy is given by $F(\eta) = E(\eta) - T[S_1(\eta) + S_i(\eta)]$ as specified by eqs. (18), (21), and (24). For simplicity we now specialize to the case of the half-filled band, $n = 1$. We then find

$$\frac{F(\eta)}{WN} = -\left(\frac{2k_BT}{W} \right) (1 - \Phi) \ln \cosh \left(\frac{W\Phi}{4k_BT} \right) - \left(\frac{2k_BT}{W} \right) \Phi \ln 2 - \left(\frac{2k_BT}{W} \right) \left[(2\Phi - 1) \int_0^1 dx \ln \cosh \left(\frac{W\Phi x}{4k_BT} \right) \right] + \left(\frac{U}{W} \right) \eta - k_BT (1 - \Phi) \left\{ (1 - 2\eta) \ln \left[\frac{2}{(1 - 2\eta)} \right] - 2\eta \ln \eta \right\} \quad \ldots(25)$$

in which

$$\Phi(\eta) = 8\eta(1 - 2\eta) \quad \ldots(26)$$

Clearly, the above expression is a functional in the extrathermodynamic variable η. We obtain the actual free energy by minimizing the functional through the constraint $\partial F(\eta)/\partial\eta = 0$. This provides the following condition on η :—

$$\left(\frac{2k_BT}{W}\right)\left(\frac{\Phi'}{\Phi}\right)(1-\Phi)\ln\cosh\left(\frac{W\Phi}{4k_BT}\right)-\left[(1-\Phi)\frac{\Phi'}{2}\right]\tanh\left(\frac{W\Phi}{4k_BT}\right)$$
$$-\left(\frac{2k_BT\Phi'}{W}\right)\ln 2-\left(\frac{2k_BT}{W}\right)\left(\frac{\Phi'}{\Phi}\right)\int_0^1 dx\ln\cosh\left(\frac{W\Phi x}{4k_BT}\right)$$
$$+\left(\frac{k_BT\Phi'}{W}\right)\left[(1-2\eta)\ln\left(\frac{2}{(1-2\eta)}\right)-2\eta\ln\eta\right]$$
$$+\left[2k_BT\frac{(1-\Phi)}{W}\right]\ln\left(\frac{2\eta}{(1-2\eta)}\right)+\frac{U}{W}=0 \qquad ...(27)$$

This expression specifies the local extremum $\eta = \eta\,(k_BT/W, U/W)$ of the free energy F, which is found by substitution of the extremum point into eq. (25).

Obviously, numerical techniques are required to obtain specific predictions. We briefly cite some of the results below.

E. Numerical Predictions Concerning Double Occupancies

The fraction of doubly occupied sites η is a measure of the equilibrium density of charge carriers per site available for charge transport, since on the average there is one electron per site for $n = 1$. Eq. (27) is used to determine $\log\eta$ as a function of W/k_BT for various choices of U/W. The results are shown in Fig. 6 as a plot of $\log\eta$ *vs.* W/k_BT. As is seen, η varies only very slightly with T for $1.5 \leqslant U/W \leqslant 1.64$ and remains at a value close of 5×10^{-2}, so that $\Phi \simeq 0.4$; the material is a correlated metal. For $1.646 < U/W < 1.765$, the system undergoes two first order changes consistent with reentrant metallic characteristics. In an intermediate temperature range the material displays semiconducting characteristics; the range of stability of the PI phase increases with increasing U/W but the slope of the Arrhenius plot remains essentially unaltered. The corresponding variation just above the critical point (see below) of $U/W = 1.765$ is shown in Fig. 6(*b*); it is seen that the first-order PI → PM′ transition at higher temperatures has given way to a smooth transformation from semiconducting to metallic behaviour.

The situation is radically different for $U/W \geqslant 2$. In this case an Arrhenius plot corresponding to Figs. 6(*a*) and (*b*) simply yields a set of straight lines of increasing negative slope and with increasingly negative intercepts as U/W is increased.

F. Thermodynamic Properties of the Correlated Electron System

One can now determine the reduced free energy F/NW from eq. (25) as a function of the reduced temperature k_BT/W for various assumed U/W. The results may be summarized as follows : When $U/W \leqslant 1.646$ one obtains only one solution

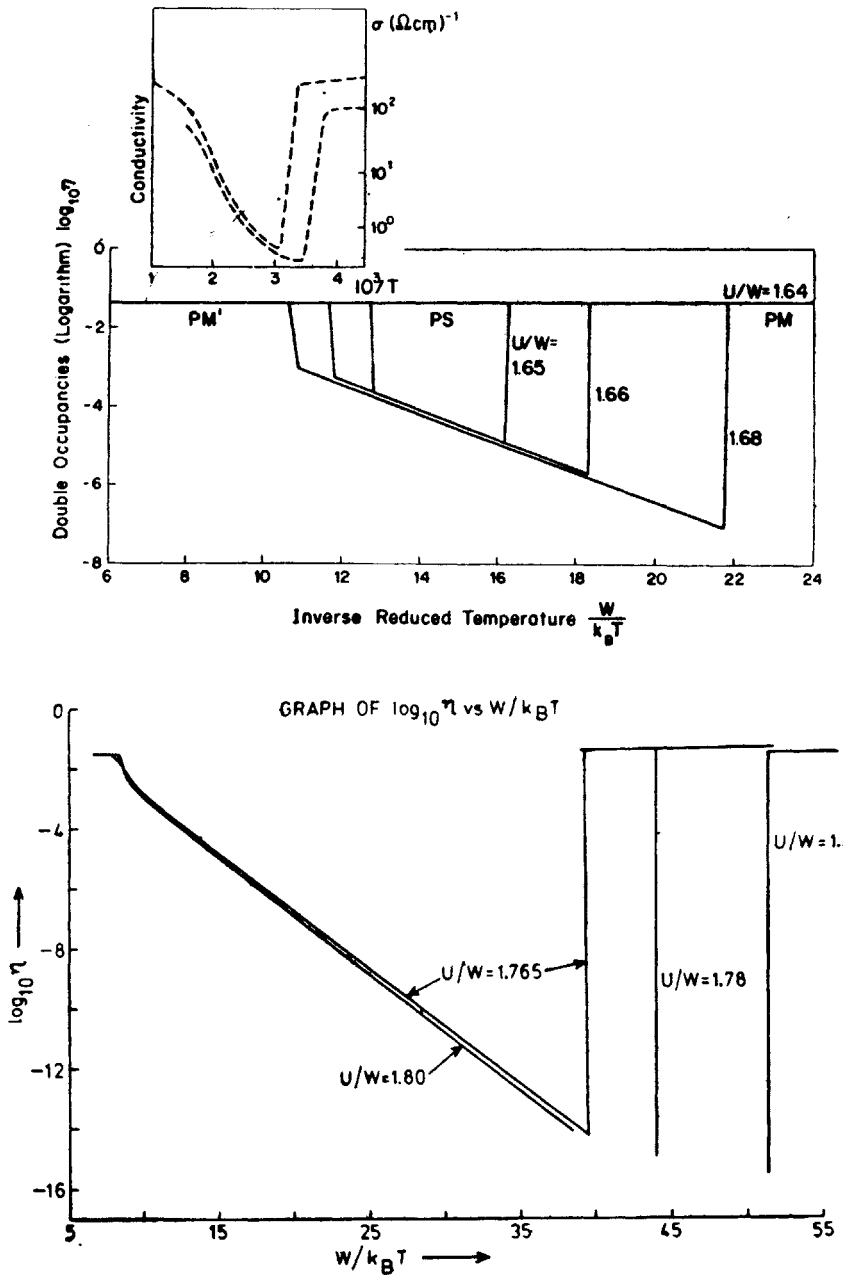

FIG 6 Plots of log η *vs* W/k_BT as determined *via* eqs. (24) and (25, 26). Part (*a*): $U/W < 1{\cdot}765$; note the two sharp electrical transitions and the intermediate PI phase whose domain shrinks as $U/W \to 1.646$. Inset shows experimental parts of log σ *vs* $10^3/T$, where σ is the conductivity of $(V_{1-x}Cr_x)_2O_3$ with $x = 0.006, 0.01$. Part (*b*): U/W slightly in excess of 1.765; note the smooth PI—PM' transition. Calculations performed for a nondegenerate half-filled band, and for a rectangular DOS.

for which F/NW diminishes roughly as $(k_BT/W)^2$ with increasing reduced temperature. For $U/W > 2$ one obtains in first approximation the result $F/WN = -(k_BT/W)\ln 2$. Both these features mirror the results obtained on the basis of the zero order theory.

In the intermediate range of U/W values one generally encounters three solutions for F/NW, of which the lower two must be examined. Obviously, the only stable solution is that for which the reduced free energy is the smallest, but there exists at least one or, over much of the range, two points where crossovers occur, precisely at the values of k_BT/W, where η exhibits the discontinuities shown in Fig. 6. These crossing point signal the occurrence of first order phase transformations; from the difference in slope of the free energy curves at the crossovers one can determine the entropy change at the transition using the thermodynamic relation $S = \partial F/\partial T$.

In Fig. 7, we show the phase diagram obtained on the basis of the crossover points described above; these results may be compared with those of Fig. 4. The more sophisticated approach automatically provides a cutoff to the upper branch of the phase boundary which lies above the critical point associated with $(U/W)_{pc}$. At low reduced temperatures the phase boundaries of Figs. 4 and 7 approach each other. The reentrant feature for the paramagnetic regime is again in evidence. For any fixed U/W in the range 1.646 to 1.765, a rise in temperature brings about a succession of changes PM → PI → PM′; the stability range of the PI phase broadens as U/W is increased. For any fixed U/W in the range 1.765 to 2 only the PM → PI phase transition is seen. For $U/W > 2$ one encounters a Mott insulator; with $U/W < 1.646$ the material remains in a correlated metallic state.

The entropy changes at the two transition points PM → PI and PI → PM′ are shown in Figs. 8(*a*) and (*b*) as plots of $\Delta S/k_BN$ *vs.* U/W. These are calculated from the difference in slopes of the corresponding free energy curves at their respective intersection points. It is seen that for both the low and the high temperature transformations the entropy discontinuity at the first order transition reaches a maximum near the midpoint of the U/W range where the transition is encountered.

V Magnetic Ordering Effects

A. The Hamiltonian of an Ordered Antiferromagnetic System

We now turn to the description of magnetic ordering effects in strongly correlated electron systems; we then show how to incorporate the essential features into the phase diagram.

We begin with the Hamiltonian for an antiferromagnetically ordered array in a which cation subarrays A and B contain atomic constituents with spins oriented in the 'up' and 'down' configurations. The total Hamiltonian may be written as

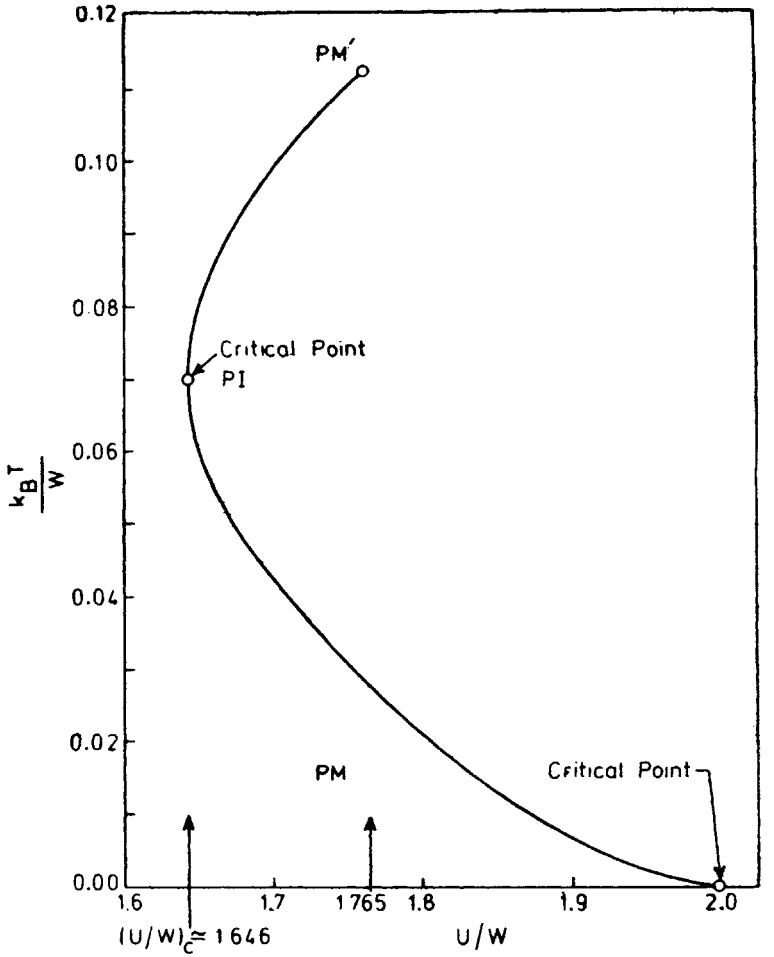

FIG 7 Improved phase diagram, based on the use of eqs. (24), (25) and (26); compare with Fig. 4. Calculations carried out for a nondegenerate, half-filled band with a rectangular DOS.

$$H = \Phi \sum_{\mathbf{k}\sigma} \epsilon_{\mathbf{k}} n_{\mathbf{k}\sigma} + U\eta + J \sum_{j \in A} \sum_{\substack{j'(j) \\ j' \in B}} (\mathbf{S}_{A_j} \cdot \mathbf{S}_{B_{j'}}) - \left(\frac{1}{4}\right) \nu_{A_j} \nu_{B_{j'}}$$

$$= H_B + U\eta + H_{ex}, \qquad \ldots(28)$$

where the last term on the right is the well-known Anderson exchange term[37] with $J = 4t^2 (1 - \Phi)/U$. As usual, we restrict the site summation j' to nearest neighbour pairs; S is a spin operator.

We proceed immediately to the mean-field approximation (derived from the assumption that $[\mathbf{a} - \langle \mathbf{a} \rangle] \cdot [\mathbf{b} - \langle \mathbf{b} \rangle] \simeq 0$)

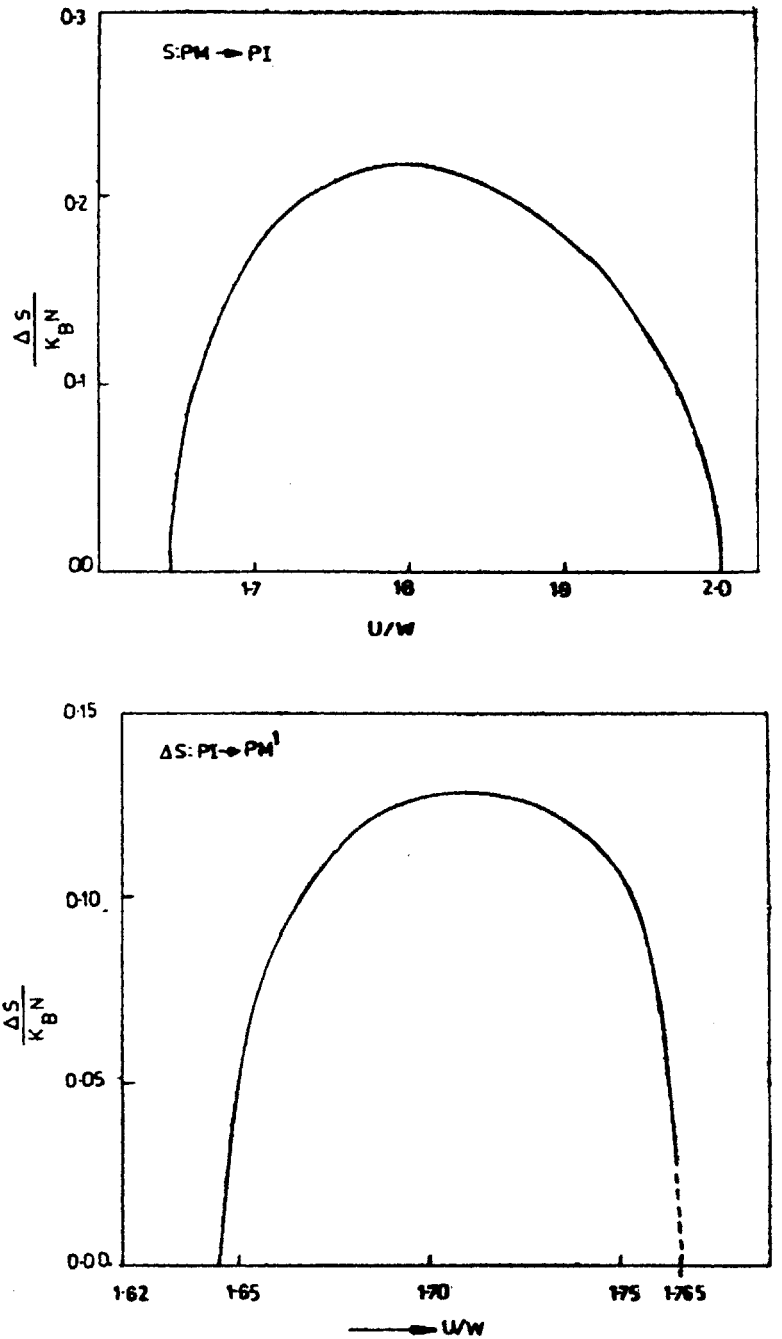

FIG 8 Plots of the reduced entropy discontinuity predicted at the first order phase transformations. Part (*a*) PM–PI transition. Part (*b*) PI–PM′ transition. Note that away from the critical U/W points the size of the entropy discontinuity peaks near the centre of the range in U/W where fist order phase changes occur.

$$\mathbf{S}_{Aj}\cdot\mathbf{S}_{Bj'} \simeq \langle\mathbf{S}_{Aj}\rangle\cdot\mathbf{S}_{Bj'} + \langle\mathbf{S}_{Bj'}\rangle\cdot\mathbf{S}_{Aj} - \langle\mathbf{S}_{Aj}\rangle\cdot\langle\mathbf{S}_{Bj'}\rangle \qquad ...(29)$$

$$\nu_{Aj}\nu_{Bj'} \cong \langle\nu_{Aj}\rangle\nu_{Bj'} + \langle\nu_{Bj'}\rangle\nu_{Aj} - \langle\nu_{Aj}\rangle\langle\nu_{Bj'}\rangle \qquad ...(30)$$

Let the magnetization be along the z-axis; then $\mathbf{S}_{Aj}\cdot\langle\mathbf{S}_{Bj'}\rangle = S^z_{Aj}\langle S^z_{Bj'}\rangle$ and $\langle S^z_{Aj}\rangle = -\langle S^z_{Bj'}\rangle = \langle S^z\rangle$. Also, $\langle\nu_{Aj}\rangle = \langle\nu_{Bj}\rangle \equiv \nu$. On inserting these results into the last term of eq. (28) and carrying out the indicated summations, we find

$$H_{ex} = -JZ\langle S^z\rangle\Big[\sum_{j\in A} S^z_{Aj} - \sum_{\substack{j'\in B\\ j'(j)}} S^z_{Bj'}\Big] + JZ\langle S^z\rangle^2\frac{N}{2}$$

$$-\frac{J}{4}Z\Big\{\sum_{j\in A} 2\nu\nu_{Aj} - \frac{N}{2}\nu^2\Big\}. \qquad ...(31)$$

Conservation laws [(eq. 2) with $n = 1$] require that $\nu \equiv \langle\nu_{Aj}\rangle = 1 - 2\langle\eta_{Aj}\rangle \equiv 1 - 2\eta$. We also invoke the invariance requirement $\eta_{Aj} = \eta$, so that $\nu_{Aj} = 1 - 2\eta_{Aj} = 1 - 2\eta$; then eq. (31) becomes

$$H_{ex} = -JZ\langle S^z\rangle\Big[\sum_{j\in A} S^z_{Aj} - \sum_{\substack{j'\in B\\ j'(j)}} S^z_{Bj'}\Big] + JZ\langle S^z\rangle^2\frac{N}{2}$$

$$-\frac{JZ}{8}N(1-2\eta)^2 \qquad ...(32)$$

Next we introduce second quantization through the relations

$$S^z_j = \tfrac{1}{2}(n_{j\sigma} - n_{j-\sigma}) = \tfrac{1}{2}\sum_{\sigma}\sigma n_{j\sigma} \quad (\sigma = \pm 1), \qquad ...(33)$$

wherein $n_{j\sigma}$ is the number operator with a value of 0 or 1 according as site j is not or is occupied by an electron of spin σ; the factor $\frac{1}{2}$ arises because in units of $\hbar$ the electron spin has the value $\pm\frac{1}{2}$. Then eq. (32) becomes

$$H_{ex} = \tfrac{1}{2}JZ\langle S^z\rangle\Big[\sum_{\substack{j'\in B\\ \sigma}}\sigma n_{Bj'\sigma} - \sum_{\substack{j\in A\\ \sigma}}\sigma n_{Aj\sigma}\Big] + JZ\langle S^z\rangle^2\frac{N}{2}$$

$$-\frac{JZN}{8}(1-2\eta)^2 \qquad ...(34)$$

At this point, it is expedient to introduce the Fourier transformation which converts creation and annihilation operators for direct space into corresponding quantities in reciprocal space.

$$a^+_{Aj\sigma} = \Big(\frac{N}{2}\Big)^{-1/2}\sum_{\mathbf{k}} a^+_{\mathbf{k}\sigma}\, e^{i\mathbf{k}.\mathbf{R}_j} \quad a_{Aj\sigma} = \Big(\frac{N}{2}\Big)^{-1/2}\sum_{\mathbf{k}'} a_{A\mathbf{k}'\sigma}\, e^{-i\mathbf{k}'.\mathbf{R}_j}$$

...(35)

By use of lattice sum rules it is then a straightforward exercise to show that $\sum_{j\in A}$ $\sum_{\sigma} \sigma n_{Aj\sigma} = \sum_{\mathbf{k}} \sum_{\sigma} \sigma n_{A\mathbf{k}\sigma}$, whence,

$$H_{ex} = \tfrac{1}{2} JZ \langle S^z \rangle \left[\sum_{\mathbf{k}\sigma} \sigma(n_{B\mathbf{k}\sigma} - n_{A\mathbf{k}\sigma}) \right] + \frac{JZ \langle S^z \rangle^2 . N}{2}$$

$$- \frac{JZN}{8} (1 - 2\eta)^2 \qquad \ldots(36)$$

We next turn our attention to the band energy term H_B in eq. (28); however, to distinguish between itinerant electrons on A and B sublattices we must first transform back from reciprocal to real space, using transformations inverse to eq. (35) One can show without difficulty that this operation leads to

$$H_B \equiv \Phi \sum_{\mathbf{k}\sigma} \epsilon_{\mathbf{k}} a^+_{\mathbf{k}\sigma} a_{\mathbf{k}\sigma} = \Phi \sum_{\sigma} \sum_{\substack{j'(j) \\ j}} t_{jj'} a^+_{j\sigma} a_{j'\sigma} \qquad \ldots(37)$$

with

$$t_{jj'} \equiv \left(\frac{N}{2}\right)^{-1} \sum_{\mathbf{k}} \epsilon_{\mathbf{k}} \, e^{i\mathbf{k}.(\mathbf{R}j - \mathbf{R}j')} \qquad \ldots(38)$$

which permits one first to generalize eq. (37) to a two-sublattice system

$$H_B = \Phi \sum_{\sigma} \sum_{j'(j)} \mathrm{t}_{jj'} (a^+_{Aj\sigma} a_{Bj'\sigma} + a^+_{Bj\sigma} a_{Aj'\sigma}) \qquad \ldots(39)$$

and then once more to switch back to reciprocal space *via* eqs. (35). When the term so obtained is inserted for H_B, and after eq. (36) is used for H_{eq}, eq. (28) reduces to the final form

$$H = \sum_{\mathbf{k}\sigma} \{E_{\mathbf{k}} (a^+_{A\mathbf{k}\sigma} a_{B\mathbf{k}\sigma} + a^+_{B\mathbf{k}\sigma} a_{A\mathbf{k}\sigma} + \sigma\Delta (n_{B\mathbf{k}\sigma} - n_{A\mathbf{k}\sigma}\}$$

$$+ U\eta + JZ \langle S^z \rangle^2 \left(\frac{N}{2}\right) - JZN \frac{(1 - 2\eta)^2}{8} \equiv H_I + U\eta + H_M \qquad \ldots(40)$$

with

$$\Delta \equiv \frac{JZ \langle S^z \rangle}{2} \text{ and } E_{\mathbf{k}} \equiv \Phi\epsilon_{\mathbf{k}}. \qquad \ldots(41)$$

Eq. (40) must now be diagonalized. A very useful standard procedure in such a situation involves the so-called *Bogolyubov transformation* :

$$a^+_{A\mathbf{k}\sigma} = u_{\mathbf{k}} \alpha^+_{1\mathbf{k}\sigma} + v_{\mathbf{k}} \alpha^+_{2\mathbf{k}\sigma} \qquad \ldots(42)$$

$$a^+_{B\mathbf{k}\sigma} = - v_{\mathbf{k}} \alpha^+_{1\mathbf{k}\sigma} + u_{\mathbf{k}} \alpha^+_{2\mathbf{k}\sigma} \qquad \ldots(43)$$

in which $\alpha^+_{1\mathbf{k}\sigma}, \alpha^+_{2\mathbf{k}\sigma}$ replace the original operators $a^+_{A\mathbf{k}\sigma}, a^+_{B\mathbf{k}\sigma}$; the transformation set (42, 43) is unitary in that $u^2_{\mathbf{k}} + v^2_{\mathbf{k}} = 1$. It is a very straightforward but tedious procedure to substitute (42) and (43) for the operators in eq. (40) and to collect terms. After appropriate manipulations one obtains (we have suppressed some subscripts on α)

$$H_I = \sum_{\mathbf{k}\sigma} \{[-2E_{\mathbf{k}} u_{\mathbf{k}} v_{\mathbf{k}} - \sigma\Delta(u^2_{\mathbf{k}} - v^2_{\mathbf{k}})]\, \alpha^+_1\alpha_1 + [2E_{\mathbf{k}} u_{\mathbf{k}} v_{\mathbf{k}} + \sigma\Delta(u^2_{\mathbf{k}} - v^2_{\mathbf{k}})]\, \alpha^+_2\alpha_2 + (E_{\mathbf{k}}(u^2_{\mathbf{k}} - v^2_{\mathbf{k}}) - 2\sigma u_{\mathbf{k}} v_{\mathbf{k}} \Delta)(\alpha^+_1\alpha_2 + \alpha^+_2\alpha_1)\} \quad \ldots(44)$$

Without loss of generality one may require the multiplier of $(\alpha^+_1\alpha_2 + \alpha^+_2\alpha_1)$ to vanish which immediately diagonalizes H_I and thereby identifies the eigenvalues from the multipliers of $\alpha^+_1\alpha_1$ and of $\alpha^+_2\alpha_2$. For further ease of manipulation we set $u_{\mathbf{k}} \equiv \cos\theta_{\mathbf{k}}$, $v_{\mathbf{k}} \equiv \sin\theta_{\mathbf{k}}$; the vanishing of the multiplier in line 2 of eq. (44) together with $\cos^2(2\theta_{\mathbf{k}}) + \sin^2(2\theta_{\mathbf{k}}) = 1$, yields

$$\sin(2\theta_{\mathbf{k}}) = \pm \frac{E_{\mathbf{k}}}{[E^2_{\mathbf{k}} + \Delta^2]^{1/2}} \qquad \cos(2\theta_{\mathbf{k}}) = \pm \frac{\Delta}{[E^2_{\mathbf{k}} + \Delta^2]^{1/2}}. \quad \ldots(45)$$

The eigenvalues are now given by

$$E_{1\mathbf{k}} = -E_{2\mathbf{k}} = -2E_{\mathbf{k}} u_{\mathbf{k}} v_{\mathbf{k}} - \sigma(u^2_{\mathbf{k}} - v^2_{\mathbf{k}})\Delta = -[E^2_{\mathbf{k}} + \Delta^2]^{1/2} \quad \ldots(46)$$

in which we have kept as mutually consistent only the solution for which $\sigma = +1$.[36] As usual, the $N/2$ successive quantized $E_{\mathbf{k}}$ values are so closely spaced that they may be regarded as quasi-continuous. One should observe that the magnetic ordering phenomena cause a splitting of the band into two parts, $+[E^2 + \Delta^2]^{1/2}$ and $-[E^2 + \Delta^2]^{1/2}$, with a gap of $2\Delta = JZ\langle S^z\rangle$; for large E the dispersion relation becomes nearly linear.

B. Magnetization Effects

Our next task is to determine the net magnetization of the system in terms of the dimensionless parameter J/W. For this purpose we set up the expectation value $\langle S^z\rangle$ at zero temperature;

$$\langle S^z\rangle + \tfrac{1}{2}\frac{1}{N/2}\sum_{j\in A}(n_{Aj\sigma} - n_{Aj-\sigma}) \equiv \frac{1}{N}\sum_{\mathbf{k}\sigma}\sigma a^+_{A\mathbf{k}\sigma} a_{A\mathbf{k}\sigma}. \quad \ldots(47)$$

On introducing the Bogolyubov transformation we find

$$\langle S^z\rangle = \left(\frac{1}{N}\right)\sum_{\mathbf{k}\sigma}\sigma\langle(u_{\mathbf{k}}\alpha^+_{1\mathbf{k}\sigma} + v_{\mathbf{k}}\alpha^+_{2\mathbf{k}\sigma})(u_{\mathbf{k}}\alpha_{1\mathbf{k}\sigma} + v_{\mathbf{k}}\alpha_{2\mathbf{k}\sigma})\rangle$$

$$= \left(\frac{1}{N}\right) \sum_{\mathbf{k}\sigma} \sigma[u_{\mathbf{k}}^2 \langle \alpha_{1\mathbf{k}\sigma}^{+} \alpha_{1\mathbf{k}\sigma} \rangle + v_{\mathbf{k}}^2 \langle \alpha_{2\mathbf{k}\sigma}^{+} \alpha_{2\mathbf{k}\sigma} \rangle] \qquad \ldots(48)$$

in which the cross term in $\langle \alpha_1^{+}\alpha_2 + \alpha_2^{+}\alpha_1 \rangle$ was dropped since the Hamiltonia is already diagonalized. As before, we set $u_{\mathbf{k}} = \cos\theta_{\mathbf{k}}$, $v_{\mathbf{k}} = \sin\theta_{\mathbf{k}}$ and introduce eq. (45) to obtain

$$\langle S^z \rangle = \frac{1}{N} \sum_{\mathbf{k}\sigma} \tfrac{1}{2}\sigma \left\{ \left[1 + \frac{\sigma\Delta}{(E_{\mathbf{k}}^2 + \Delta^2)^{1/2}} \right] \langle \alpha_{1\mathbf{k}\sigma}^{+} \alpha_{1\mathbf{k}\sigma} \right.$$

$$\left. + \left[1 - \frac{\sigma\Delta}{(E_{\mathbf{k}}^2 + \Delta^2)^{1/2}} \right] \langle \alpha_{2\mathbf{k}\sigma}^{+} \alpha_{\mathbf{k}\sigma} \rangle \right\} \qquad \ldots(49)$$

On summing over σ, introducing $\Delta = (\frac{1}{2})\, JZ \langle S^z \rangle$, and using Fermi-Dirac statistics (i.e. the Fermi-Dirac Function (51) to replace expectation values of the operators we find

$$1 = \tfrac{1}{2} \frac{JZ}{N} \sum_{\mathbf{k}} \frac{f_{1\mathbf{k}} - f_{2\mathbf{k}}}{(E_{\mathbf{k}}^2 + \Delta^2)^{1/2}} \qquad \ldots(50)$$

Now set $q_{\mathbf{k}} \equiv (E_{\mathbf{k}}^2 + \Delta^2)^{1/2}/k_B T$. Then the Fermi-Dirac Function becomes

$$f_{1,2\mathbf{k}} = f\left[\pm \frac{(E_{\mathbf{k}}^2 + \Delta^2)}{k_B T} \right] = \frac{1}{\exp(\pm q_{\mathbf{k}}) + 1} \qquad \ldots(51)$$

so that eq. (50) may be written as

$$1 = \tfrac{1}{2} \frac{JZ}{N} \sum_{\mathbf{k}} \frac{1}{(E_{\mathbf{k}}^2 + \Delta^2)^{1/2}} \left\{ \frac{1}{\exp(-q_{\mathbf{k}}) + 1} - \frac{1}{\exp(q_{\mathbf{k}}) + 1} \right\}$$

$$= \tfrac{1}{2} \frac{JZ}{N} \sum_{\mathbf{k}} \frac{\tanh(q_{\mathbf{k}}/2)}{(E_{\mathbf{k}}^2 + \Delta^2)^{1/2}} \qquad \ldots(52)$$

Next, introduce the scaling law $E_{\mathbf{k}} = \Phi\epsilon_{\mathbf{k}}$ as before and change to an integration. As usual, the summation is replaced by $\left(\frac{N}{2}\right) \int \mathrm{d}\epsilon \sum_{\mathbf{k}} \delta(\epsilon - \epsilon_{\mathbf{k}})\, \rho_0^{\sigma}(\epsilon)$. This yields

$$1 = \frac{JZ}{4} \int_{-W/2}^{W/2} \mathrm{d}\epsilon\, \rho_0^{\sigma}(\epsilon) \frac{\tanh(q_{\mathbf{k}}/2)}{[\epsilon_{\mathbf{k}}^2 \Phi^2 + \Delta^2]^{1/2}} \qquad \ldots(53)$$

For the conventional rectangular DOS we find

$$1 = \frac{JZ}{2W\Phi} \int_{0}^{W\Phi/2} \mathrm{d}E\, \frac{\tanh(q_{\mathbf{k}}/2)}{(E_{\mathbf{k}}^2 + \Delta^2)^{1/2}} \qquad \ldots(54)$$

The integral may be evaluated for $\Phi \ll 1$ using Rolle's theory of the mean to obtain

$$1 = \frac{JZ}{4} \frac{\tanh \{[(W\Phi/4)^2 + \Delta^2]^{1/2}/2k_BT\}}{[(W\Phi/4)^2 + \Delta^2]^{1/2}} \qquad ...(55)$$

and in the limit $\Phi \to 0$ and with $\Delta = JZ \langle S^z \rangle/2$ this reduces to

$$\langle S^z \rangle = \tfrac{1}{2} \tanh \left[\frac{JZ \langle S^z \rangle}{4k_BT} \right] \qquad ...(56)$$

C. The Ground State Energy

The ground state energy is specified by the expression

$$\frac{E_G}{N} = \left(\frac{1}{N}\right) \sum_{\mathbf{k}\sigma} \{E_{1\mathbf{k}} \langle \alpha^+_{1\mathbf{k}\sigma} \alpha_{1\mathbf{k}\sigma} \rangle + E_{2\mathbf{k}} \langle \alpha^+_{2\mathbf{k}\sigma} \alpha_{2\mathbf{k}\sigma} \rangle\}$$

$$- \left(\frac{JZ}{8}\right)(1 - 2\eta)^2 + U\eta + \frac{JZ \langle S^z \rangle^2}{2} \qquad ...(57)$$

We now replace the two expectation values of the operators by $f_{1\mathbf{k}}, f_{2\mathbf{k}}$ as given by eq. (51) and we introduce (46). After considerable, through straightforward simplification the summation term yields

$$\frac{E_B}{N} = -\left(\frac{2}{N}\right) \sum_{\mathbf{k}} k_BT\, q_{\mathbf{k}} \tanh \left(\frac{q_{\mathbf{k}}}{2}\right) \qquad ...(58)$$

We next switch to an integration to replace the summation, using the same procedure as in Sec. IVB. We also introduce the conventional rectangular DOS. Then the summation term reads

$$\frac{E_B}{N} = -\left(\frac{2}{W}\right) \int_0^{W/2} \mathrm{d}\epsilon\, [(\Phi\epsilon_{\mathbf{k}})^2 + \Delta^2]^{1/2} \tanh \left\{ \frac{[(\Phi\epsilon_{\mathbf{k}})^2 + \Delta^2]^{1/2}}{2k_BT} \right\} \qquad ...(59)$$

For $\Phi \ll 1$, the integral may be evaluated by using Rolle's theorem, which leads to

$$\frac{E_B}{N} = -\left[\left(\frac{\Phi W}{4}\right)^2 + \Delta^2\right]^{1/2} \tanh \left\{ \frac{[(\Phi W/4)^2 + \Delta^2]^{1/2}}{2k_BT} \right\} \qquad ...(60)$$

and as $\Phi \to 0$ this simplifies to

$$\frac{E_B}{N} = -\left(\frac{JZ \langle S^z \rangle}{2}\right) \tanh \left(\frac{JZ \langle S^z \rangle}{4k_BT}\right) \qquad ...(61)$$

Finally, introducing eq. (56) one finds the simple expression

$$\frac{E_B}{N} = -JZ \langle S^z \rangle^2 \simeq -\frac{JZ}{4}, \qquad ...(62)$$

where the term on the right is a limiting case at low temperature : in the mean field approximation $\langle S^z \rangle = \frac{1}{2}$ (in units of $\hbar$). The ground state energy in this approximation is found from eq. (57) to be

$$\frac{E_G}{N} = -\frac{JZ}{4}, \qquad \ldots(63)$$

where we have set $\eta = 0$, consistent with the earlier approximation of taking $\Phi = 0$.

D. The AFI-PM Transition

At this stage we can inquire under what circumstances a transition from the antiferromagnetic insulating state to the correlated metallic state can take place. The necessary and sufficient condition is that $(F/N)_{\mathrm{AFI}} = (F/N)_{\mathrm{PM}}$. For the AFI phase we use a drastic simplifying assumption; namely, we equate F/N with E_G/N, as given by eq. (63); for, as is well established, the entropy contributions to the free energy of the magnetically ordered insulator are small in the low temperature range for which the derivation leading to (63) is valid. Furthermore, we neglect any changes in W arising from magnetic ordering effects. Eq. (11) specifies the chemical potential for the correlated metal. On (*i*) equating these relations, (*ii*) introducing the expression $\Phi = 1 - (U/2W)^2$, and (*iii*) the formulation $\eta = (1/4)\ (1 - U/2W)$, both valid at low temperatures for the PM phase, one can solve for

$$\frac{k_B T}{W} = \left\{\frac{3\Phi}{\pi}\left[\frac{JZ}{4W} - \tfrac{1}{4}\left(1 - \frac{U}{2W}\right)^2\right]\right\}^{1/2} \qquad \ldots(64)$$

which represents the equation for the reduced antiferromagnetic transition temperature in its dependence on the U/W parameter. This relation with $J = 4t^2 (1 - \Phi)/U$ and $t = W/2Z$, $Z = 4$ is sketched as the lower left curve for the phase diagram, Fig. 9.

E. *The AFI-PI Transition*

An analysis comparable to that of the preceding Section may now be carried out to establish the phase boundary separating the AFI and PI phases. For this purpose we equate E_G/N, eq. (63), with F_{PI}/N as read off from eq. (13). Once again, one must bear in mind the many approximations that are invoked to arrive at these limiting expressions. The final result is specified by

$$\frac{k_B T}{W} = \frac{JZ}{4} \ln 2 \qquad \ldots(65)$$

with $J = 4t^2 (1 - \Phi)/U$ and $t = W/2Z$, $Z = 4$ as before. A plot of $k_B T/W$ *vs.* U/W resulting from the above is shown as the lower right curve in Fig. 9.

VI Discussion

The final theoretical phase diagram is exhibited in Fig. 9 for the theory developed in Secs. VD and VE. One should first recall again the many restrictions and

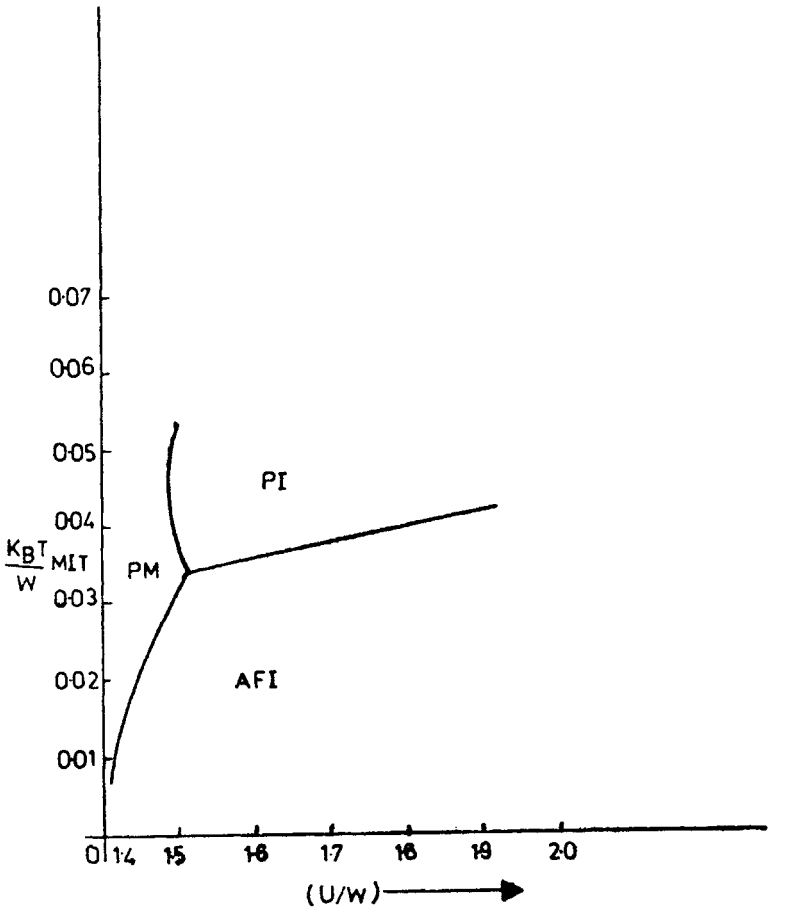

FIG 9 Final form of the theoretical phase diagram in the low temperature approximation as developed in Sec. VD and VE. Note the triple point. For the higher-temperature paramagnetic regime in excess of $(k_BT/W)_t$ the more exact theory leading to the results of Fig. 7 must be used.

assumptions that led to this formulation : The theory is based on the existence of a nondegenerate band that is exactly half-filled; a single scaling function Φ was used to relate the energies $E_{\mathbf{k}}$ and $\epsilon_{\mathbf{k}}$ of the quasiparticles and of the bare particles; electron interactions are simulated by the single parameter U; a rectangular DOS was invoked to evaluate the integrals specifying band energies in the PM and PI phases; the low temperature limiting form was invoked and, in particular, the energy of the AFI phase was used as an approximation to the actual free energy of the magnetically ordered insulator.

One should clearly recognize that the results leading to Fig. 9 really only apply in the limit $T \to 0$, and already differ significantly from the more sophisticated theory of Sec. IV in which the limiting case $T \to 0$ is not invoked. Unfortunately,

at the time of writting, the corresponding more sophisticated theoretical calculations pertaining to the AFI → PM and AFI → PI transitions were not yet available. Thus, the phase diagram of Fig. 9 is to be regarded as an approximation to the results anticipated for the improved theories that are not based on the limit $T \to 0$. Subject to these limitations one encounters a triple point at $k_BT/W \simeq 0.034$, $U/W \simeq 1.515$ for the coexistence of the AFI, PM and PI phase. The phase boundaries for the paramagnetic regime at reduced temperatures in excess of 0.034 are to be read off from Fig. 7, based on the improved theory of Sec. IVD.

Despite all of the simplifications that have been introduced at various stages the theory does provide a relatively good account of the properties of the $(V_{1-x}Cr_x)_2O_3$ alloy system. In particular, it is evident that all the cases discussed in Sec. I have their theoretical counterpart in the phase diagrams of Fig 7 and Fig. 9; depending on the value of U/W which a adopted one may encounter zero, one, two, or three transitions when the temperature is altered. Only so long as U/W remains above a critical value (which is temperature-dependent and which approaches $(U/W)_{cr} = 2$ as $T \to 0$ for a rectangular DOS) does one deal with a case where itinerant electrons are absent from the system; such a solid is a Mott-type insulator in the sense originally proposed by Mott.[16]

To permit a comparison to be made between the theoretical and experimental phase diagrams we now establish that U/W varies nearly linearly with the mole fraction x of Cr. To do so we adopt the virtual crystal approximation in which the Hubbard parameter U is replaced by an effective parameter U_e specified by

$$U_e = U_v(1 - x) + U_{cr}x \qquad \ldots(66)$$

A corresponding effective bandwidth, W is also required. For this purpose one may adopt the proportionality $W \sim t_{ij} \sim \exp(-\lambda R_{ij})$ involving W and the transfer integral t_{ij} between nearest neighbors i and j separated by the distance R_{ij}; λ is a scaling factor. The various transitions of the V_2O_3 system are accompanied by sizeable volume changes Δv in the unit cell volume v_0. We then write $t_{ij} \simeq \exp R^0_{ij} + A\Delta R_{ij})] = \exp\{-[R^0_{ij} + Bx(\Delta v/v_0)^{1/3}]\}$, wherein R^0_{ij} is a reference interatomic separation, and $A\Delta R_{ij}$ is the change in separation introduced by replacing a vanadium atom in location j by Cr. In accord with Vegard's law, for dilute concentrations one may anticipate that $A = Bx$ is proportional to the mole fraction of the diluent. On expanding to first order terms one obtains

$$t_{ij} \sim \{\exp(-\lambda R^0_{ij})\}\left[1 + Bx\left(\frac{\Delta v}{v_0}\right)^{1/3}\right], \qquad \ldots(67)$$

whence

$$W_e = W\left[1 + Bx\left(\frac{\Delta v}{v_0}\right)^{1/3}\right] \equiv W_v + (W_{cr} - W_v)x. \qquad \ldots(68)$$

Finally, then,

$$\left(\frac{U}{W}\right)_e = \frac{U_v + (U_{cr} - U_v)x}{W_v + (W_{cr} - W_v)x} = \frac{U_v}{W_v}\left[1 + \frac{U_{cr} - U_v}{U_v} + \frac{W_v - W_{cr}}{W_v}x\right] \qquad \ldots(69)$$

which shows explicitly the linear variation of U/W with x in the present approximation.

U/W may further be altered by the atomic potential fluctuations that arise when Cr is substituted for V. Let $\Delta\epsilon \equiv \epsilon_{Cr} - \epsilon_v < 0$ be the energy difference for an electron localized at a Cr as compared to a V atom. The expectation value of the energy is then given by $\Sigma_{(i\sigma)} E_i \langle n_{i\sigma} \rangle$, where E_i may assume the values E_{Cr} or E_v depending on the site index i. This expectation value may be simulated by the product $(1 - \Phi)\, x\Delta\epsilon$. The first factor pertains to the probability that an electron is actually localized (See Sec. IVA); the factor x represents the probability that a site containing a Cr atom is encountered. The inhomogeneity arising from the Cr substitution thus enhances localization as expressed through the factor $(1 - \Phi)$; this correction must be added to the energy contribution $-(W/U)\,\Phi$ as specified in eq. (6); we obtain an effective band energy

$$\frac{E_B}{N} = x\Delta\epsilon - \left(\frac{W}{U}\right)\left[1 + \left(\frac{4\Delta\epsilon}{W}\right)x\right]\Phi. \qquad \ldots(70)$$

Since $\Delta\epsilon < 0$, the multiplier $[1 + (4\Delta\epsilon/W)\, x]$ represents an additional band narrowing factor associated with the lattice disorder due to the random distribution of Cr atoms. This factor is a linearized form of the Anderson localization effect arising from the presence of randomly fluctuating potentials in the lattice.

The total variation of (U/W) with x is then given by the linear relationship

$$\frac{U}{W} = \frac{U_v}{W_v}\left[1 + \left(\frac{U_{Cr} - U_v}{U_v}\right) + \left(\frac{W_v - W_{Cr}}{W_v} - \frac{4\Delta\epsilon}{W_v}\right)x\right] \qquad \ldots(71)$$

The above permits k_BT/W and U/W to be replaced with k_BT/W_e and $(U/W)_e$ respectively and to be linearized as shown in eqs. (68) and (71).

One should not set too much store by the numerical values assigned to the critical points identified in Fig. 7 or 9 or to any other values which might be obtained by a fit to experimental data. These fits are all derived for the special case $n = 1$ and are sensitive to the type of DOS employed in the evaluation of the integrals specifying the band energies. The main point is that a consideration of electron correlation effects alone already provides a mechanism for a basic understanding of the set of phase transitions as well as of the reentrant metallic properties in the $(V_{1-x}Cr_x)_2O_3$ system. However, there are two important qualifications that must be carefully kept in mind.

First, the numerical predictions are somewhat off the mark. For example, the calculated entropy changes shown in Fig. 8 are too high by a factor of two relative to the experimental values cited by the Purdue group.[37a] Also, the PI → PM′ transition which is predicted to be of first order is actually spread out over a very large temperature range; if one attempts to circumvent this problem by choosing a U/W just slightly larger than the value corresponding to the upper terminal point in Fig. 7 then one does obtain a continuous PI → PM′ transition as shown in Fig. 6(*b*). However, the predicted low-temperature PM → PI transformation is too large by many orders of magnitude. Lastly, the predicted transition temperatures read off

from Fig. 7 and 9 are too high by a factor of two or three, unless one chooses unrealistically small values $W \leqslant 0.3$eV for the bare-particle band-width.

Second, there is unmistakable experimental evidence to the effect that the lattice plays an important role in the transition. This is brought out clearly in several types of experimental measurements :—

X-ray diffraction experiments[7,38] indicate that there is a sizeable expansion of the lattice during the PM → AFI and PM → PI transitions.

(ii) Raman scattering experiments[39–41] show that virtually all Raman-active modes alter in frequency during the transitions.

(iii) There are enormous hysteresis effects of ca. 50 K[14] in the PM → PI transition, and for magnetic ordering transitions that occur below 50 K.

(iv) Ultrasonic measurements[42–44] show that certain elastic constants of the alloys soften near the AFI-PI or AFI-PM phase changes.

(v) Careful X-ray studies have revealed the existence of Bragg satellite spots[45] that have been interpreted as indicating the onset of charge-density waves coincident with the PM → PI transition.

(vi) Inelastic neutron scattering experiments[46,47] have shown that low frequency longitudinal optical lattice vibrational modes are encountered in the alloy system along certain directions in reciprocal space.

The data are shown in Fig. 10; one should note the anomalies in the lower lying acoustic phonon branches. The interpretation of the splittings and the

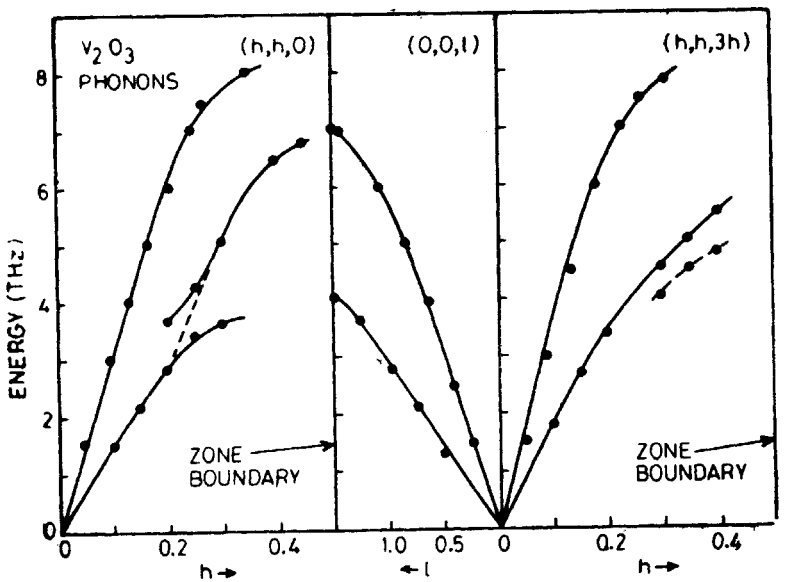

FIG 10 Acoustic phonon branch spectrum at 300 K for V_2O_3 as determined from inelastic neutron scattering experiments. Note the anomalous lower-lying branches.

presence of what may be low-lying optical modes is unclear at this point, but they are presumably correlated with peculiarities in the lattice dynamics of V_2O_3.

The above features indicate that the lattice is not passive in the initation of phase changes in the V_2O_3 alloy system. Thus, a more complete theory would require the inclusion of the energy and entropy of the lattice in the construction of the total free energy before the latter is minimized. Attempts to do so are currently in progress.

ACKNOWLEDGMENTS

The authors are greatly indebted to Ms A Datta for carrying out calculations, for a careful reading of the manuscript, and for many useful discussions. This work was supported on NSF-MRL Grant DMR 83–16988.

REFERENCES

1. M Foex *C r Acad Sci (Paris)* **223** (1946) 1126
2. F J Morin *Phys Rev Lett* **3** (1959) 34
3. J Feinleib and W Paul *Phys Rev Lett* **155** (1967) 841
4. A J MacMillan *Lab Rep Insulation Research* Massachusetts
5. D B McWhan T M Rice and J P Remeika *Phys Rev Lett* **23** (1969) 1384
6. A Menth and J P Remeika *Phys Rev* **B2** (1970) 3756
7. D B McWhan and J P Remeika *Phys Rev* **B2** (1970) 3734
8. D B McWhan A Menth and J P Remeika *J Phys (Paris)* **32** (1971a) C1–1079
9. D B McWhan A Menth J P Remeika W F Brinkman and T M Rice *Phys Rev* **B7** (1973) 1920
10. D B McWhan J P Remeika T M Rice W F Brinkman J P Maita and A Menth *Phys Rev* **27** (1971) 941
11. K Nagasawa Y Bando and T Takada *J Cryst Growth* **17** (1972) 143
12. J M Honig and L L Van Zandt In : *Annual Review of Materials Science* (*Ed* R A Huggins R N Bube and R W Roberts) *Ann Rev Proc Palo Alto* CA pp 225ff (1975)

12*a*. J M Honig G V Chandrashekhar and A P B Sinha *Phys Rev Lett* **32** (1974) 13

12*b*. A P B Sinha G V Chandrashekhar and J M Honig *J Solid State Chem* **12** (1975) 402

13. H Kuwamoto H V Keer J E Keem S A Shrivashankar L L Van Zandt and J M Honig *J Phys (Paris)* **37** (1976) C1–35
14. H Kuwamoto J M Honig and J Appel *Phys Rev* **B22** (1980) 2626
15. S A Shivashankar and J M Honig *Phys Rev* **B28** (1983) 5695
16. N F Mott *Proc phys Soc (London)* **A62** (1949) 416
17. N F Mott *J Canad Phys* **34** (1956) 1356
18. N F Mott *Phil Mag* **6** (1967) 287
19. N F Mott *Rev mod Phys* **40** (1968) 677
20. J Hubbard *Proc R Soc London* **A237** (1963) 238; *Proc R Soc London* **A281** (1964) 401
21. W F Brinkman and T M Rice *Phys Rev* **B2** (1970) 4302
22. J Spalek A M Oleś and J M Honig *Phys Rev* **B28** (1983) 6802
23. M Cyrot *J Phys (Paris)* **33** (1972) 125
24. M Cyrot and P Lacour-Gayet *Solid State Commun* **11** (1972) 997
25. T Moriya and H Hasegawa *J phys Soc Japan* **48** (1980) 1490
26. H Hasegawa *J phys Soc Japan* **49** (1980) 178

27. H J Zeiger *Phys Rev* **B11** (1975) 5123
28. M Weger *Phil Mag* **24** (1971) 1095
29. J Ashkenazi and M Weger *J Phys (Paris)* **37** (1976) C4–189
30. C Castellani C R Natoli and J Ranninger *Phys Rev* **B18** (1978) 4945, 4967 and 5001
31. M Grodzicki O Jepson O Anderson and J Appel *Unpublished Research* (1983)
32. A Minesaki *Phys Lett* **B32** (1970) 235
33. R Ramirez L M Falicov and J C Kimball *Phys Rev* **B2** (1970) 3751
34. B Alascio V Grünfeld and A Lopez *Phys Rev* **B5** (1972) 3708
35. L M Falicov and J C Kimball *Phys Rev Lett* **22** (1969) 997
36. J Spalek A Datta and J M Honig *to be published* (1985)
36*a*. J Spalek A Datta and J M Honig *Phys Rev* (1985) *in press*
37. C L Cleveland and A Rodridgo Medina *Am J Phys* **44** (1976) 44
37*a*. G M Joshi H V Keer and J M Honig *Inter J Thermophys* **1** (1980) 185
38. W R Robinson *Acta Cryst* **B31** (1975) 1153
39. N Kuroda and H Y Fan *Phys Rev* **B16** (1979) 5003
40. C Tatsuyama and H Y Fan *Phys Rev* **B21** (1980) 2977
41. A Okamoto Y Fujita and C Tatsuyama *J phys Soc Japan* **52** (1983) 312
42. D N Nichols and R J Sladek *Phys Rev* **B24** (1981) 3155
43. D N Nichols R J Sladek and H R Harrison *Phys Rev* **B24** (1981) 3025
44. H Yang R J Sladek and H R Harrison *Solid State Commun* **47** (1983) 955
45. F Sinclair and R Colella *Solid State Commun* **31** (1979) 359
46. M Yethiraj S A Werner W B Yelon and J M Honig *AIP Conf Proc* **89** (1982) 343
47. M Yethiraj S A Werner W B Yelon and J M Honig Submitted for publication (1985)